Solid State Communications 151 (2011) 688–692

Contents lists available at ScienceDirect

Solid State Communications

journal homepage: www.elsevier.com/locate/ssc

Real-time manipulation of gold nanoparticles inside a scanning electron microscope

Sergei Vlassov [a,*], Boris Polyakov [a,b], Leonid M. Dorogin [a], Ants Lõhmus [a], Alexey E. Romanov [a,c], Ilmar Kink [a,d], Enrico Gnecco [e], Rünno Lõhmus [a]

[a] Institute of Physics, University of Tartu, Riia 142, 51014, Tartu, Estonia
[b] Institute of Solid State Physics, University of Latvia, 8 Kengaraga Street, Riga, LV-1063, Latvia
[c] Ioffe Physical Technical Institute, RAS, 26 Polytekhnicheskaya, St Petersburg, 194021, Russian Federation
[d] Estonian Nanotechnology Competence Center, Riia 142, 51014, Tartu, Estonia
[e] IMDEA Nanociencia, Campus Universitario de Cantoblanco, Avda. Fco. Tomás y Valiente 7, 28049 Madrid, Spain

ARTICLE INFO

Article history:
Received 18 January 2011
Received in revised form
14 February 2011
Accepted 16 February 2011
by P. Sheng
Available online 23 February 2011

Keywords:
A. Nanostructures
A. Surfaces and interfaces
C. Scanning and transmission electron microscopy
E. Mechanical properties

ABSTRACT

The forces needed to overcome static friction and move 150 nm diameter Au nanoparticles on an oxidized Si substrate were measured in Normal and Shear oscillation modes inside a scanning electron microscope (SEM) in real time. The experimental setup consisted of a quartz tuning fork (QTF) mounted onto a high-precision 3D nanomanipulator used with a glued silicon or tungsten tip as a force sensor. Static friction was found to range from tens of nN to several hundred nN. Large variations in static friction values were related to differences in particle shape. Kinetic friction tended to be close to the detection limit and in most cases did not exceed several nN. The influence of thermal treatment in reducing the static friction of nanoparticles was considered.

1. Introduction

Nanoparticle manipulation experiments have two general purposes: contributing to the understanding of friction mechanisms by providing information about interactions at the nanoscale and practical benefits such as the development of precise 2D positioning and assembly methods for applications in nanoelectronics, digital information storage [1], etc.

The tool most commonly used for the manipulation of nanoparticles is the atomic force microscope (AFM). Several different approaches have been applied in AFM manipulation strategies. In the dynamic mode, particles can be moved during the scanning process when the amplitude of the tip oscillations is increased above a certain threshold value [2], and the frictional force is estimated from the dissipated power [3]. Increasing the scan rate above a certain value rather than increasing the oscillation amplitude yields similar results [4]. Another approach consists of switching the feedback off during manipulation [5]. In this case, the tip pushes particles and oscillations are not essential for the manipulation process; the cantilever deflection is recorded.

Particles can also be moved in contact mode. For example, Dietzel et al. [6] introduced a so-called "tip-on-top" strategy. In this method, the tip is first positioned on top of the nanoparticle approximately at its center. The nanoparticle then follows the tip motion. The measured torsional signal is directly proportional to the interfacial friction between the particle and the substrate.

AFM manipulations have certain limitations. First, there is no real-time visual feedback concerning the contact geometry or the particle position and behavior during manipulation (i.e., whether it is rolling or sliding). Only indirect conclusions can be drawn on the basis of the shape of the force curves [7]. Additionally, many AFM experiments are made in ambient conditions, meaning that a considerable amount of water is present on all surfaces under investigation, complicating the interpretation of forces.

Another problem is the "ageing" of a sample exposed to ambient conditions, resulting in sticking of the particles to the substrate [8]. Sticking increases significantly with time. Given that AFM manipulation experiments are time-consuming, adhesion can increase even within single experimental series.

To overcome these obstacles, manipulation experiments should be performed in a vacuum environment with real-time visual

* Corresponding author. Tel.: +372 55941841; fax: +372 7374723.
E-mail address: vlassovs@ut.ee (S. Vlassov).

0038-1098/$ – see front matter © 2011 Elsevier Ltd. All rights reserved.
doi:10.1016/j.ssc.2011.02.020

control. In this study, we measured the forces needed to overcome static friction and move individual 150 nm gold nanoparticles on an oxidized Si surface in dynamic mode inside a scanning electron microscope (SEM) using a quartz tuning fork (QTF)-based force sensor [9] mounted on a 3D nanomanipulator. This force sensor can oscillate perpendicularly (Normal mode) or parallel (Shear mode) to the surface. The applicabilities and peculiarities of the two modes as regards the manipulation of nanoparticles are compared and discussed.

2. Experimental

The 150 nm Au nanoparticles were purchased from *BBI International*. Oxidized silicon wafers (50 nm of thermal oxide) were purchased from *Semiconductor Wafer, Inc.* The samples were made by depositing droplets of an Au nanoparticle suspension onto the Si wafer. Samples were annealed for 1 h at 725 K prior to every experiment to remove the surfactant and decrease adhesion. A Helios NanoLab (*FEI*) field emission microscope was used to characterize the samples before and after thermal treatment.

Force sensors were constructed in a manner similar to that of Rozhok et al. [9]. An AFM cantilever with a silicon tip (*NT-MDT*) or etched 0.1 mm W wire [10] was glued to one prong of a commercially available QTF ($f_{res} = 32,768$ Hz) using conductive silver epoxy (*M.E. Taylor Engineering, Inc.*). Depending on the side to which the tip was glued, the sensor operated in the Normal mode or Shear mode. In Normal mode operation, the QTF oscillated perpendicularly to the surface in a manner similar to that for a conventional AFM (Fig. 1(a)). In Shear mode operation, the sensor oscillated parallel to the surface (Fig. 1(b)).

Force measurements were based on the fact that the oscillation amplitude of the sensor oscillating at its resonant frequency depends on the forces acting on the tip. Sensor oscillations were excited by applying alternating voltage to its electrodes using a lock-in amplifier (SR830; *Stanford Research Systems*). The amplitude of the free oscillations at the tip apex was on the order of 100 nm. The sensor also provided feedback for controlling the distance between the tip and the surface.

The quality factor (Q-factor) of the sensor was optimized (reasonably decreased) by adding small droplet of epoxy (Ecobond 286, *Emerson & Cuming*) onto one of the QTF prongs to enable a compromise between sufficient sensitivity and a short response time.

The force sensor was mounted on a 3D piezo-nanomanipulator (SLC-1720-S, *SmarAct*) and installed inside an SEM (VEGA II, *Tescan*). The SmarAct 3D nanomanipulator enables two types of movement: in the single-line scan regime (hereinafter the "scan regime"), the movements are made by expansion or contraction of the piezo-nanomanipulator to which the sensor is fastened. This regime provides an atomically smooth and accurate motion. In step regime, movements are made in a series of gradual expansions of the piezo-nanomanipulator followed by abrupt slips achieved via a sawtooth signal sent to the piezo-positioner.

When QTFs with AFM cantilevers were used, the sample and the sensor were tilted at 45° relative to the table plane to enable visual control of the manipulation procedure (Fig. 1(c), (d)). Manipulation in this case was done only along the *Y*-axis to provide an approximately constant distance between the tip and the sample. In the case of tungsten wire, the tip protruded hundreds of μm from the QTF prong and was clearly visible without tilting.

The thermal drift for given experimental setup was on the order of 0.1 nm/s and could thus be neglected within one manipulation event. Extensive custom software was developed for manipulation rather than using the standard *SmarAct* software.

All sensors were calibrated in both the *Y* and *Z* directions on reference contact AFM cantilevers [11] that had been previously calibrated by the thermal noise method [12].

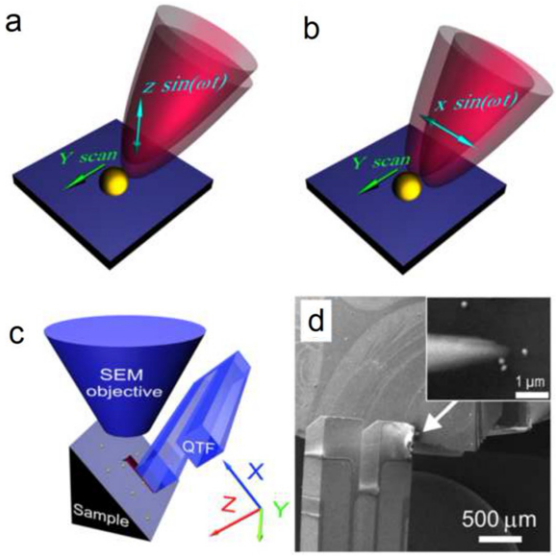

Fig. 1. Tip oscillating in (a) Normal and (b) Shear modes. (c) QTF and sample tilted at 45° to the SEM objective. (d) SEM image of the sample and QTF with the AFM tip.

For the manipulation experiment, the tip was brought into close proximity to the chosen particle. The particle was then displaced ("kicked") from its initial position by an abrupt tip motion in the step regime to reduce the initial adhesion [4], which is known to be time dependent [13], to its minimal value. Initial displacement was followed by controlled manipulation of the particle by pushing it with the tip in the scan regime with simultaneous force recording. During manipulation, the tip moved parallel to the surface along a straight line without feedback.

3. Results

Fig. 2 presents a typical manipulation curve for the QTF oscillating in Normal mode. The initial flat region **A**–**B** of the curves corresponds to the movement of the tip above the surface. The decline of the curve in region **B**–**C** was caused by a long-range interaction between the tip and the particle. The abrupt drop in amplitude at **C** corresponds to the force needed to overcome the static friction and displace the Au particle from its initial location. When static friction was overcome, the particle jumped in the direction indicated by the arrow. From **D** to **E**, the particle moved smoothly with the tip. For the moving particle, the amplitude drop was only a few percent lower than it was before contact.

Fig. 3 shows a manipulation curve for the QTF oscillating in Shear mode. The initial flat region from **A** to **B** of the curve corresponds to the movement of the tip at a constant set point above the surface. The abrupt drop in amplitude from **B** to **C** corresponds to the force needed to overcome static friction and displace the Au particle. The particle made a small jump in the direction indicated by the arrow. From **D** to **E**, the particle moved smoothly with the tip, and minor oscillations related to tip–particle interaction were noticeable.

In all manipulation experiments, the tip moved in the *Y* direction. We used the force-calibration data for the *Y* direction to convert amplitude to force (further details are given below). The static friction was found to range from 40 to 450 nN for the Normal mode and from 50 to 750 nN for the Shear mode. It should be noted that the oscillation amplitude often dropped to zero. This drop corresponds to a force higher than 1500–2500 nN (the upper limit depending on the particular sensor). Forces higher than these limits could not be measured due to the limited range of QTF sensitivity at a given driving voltage.

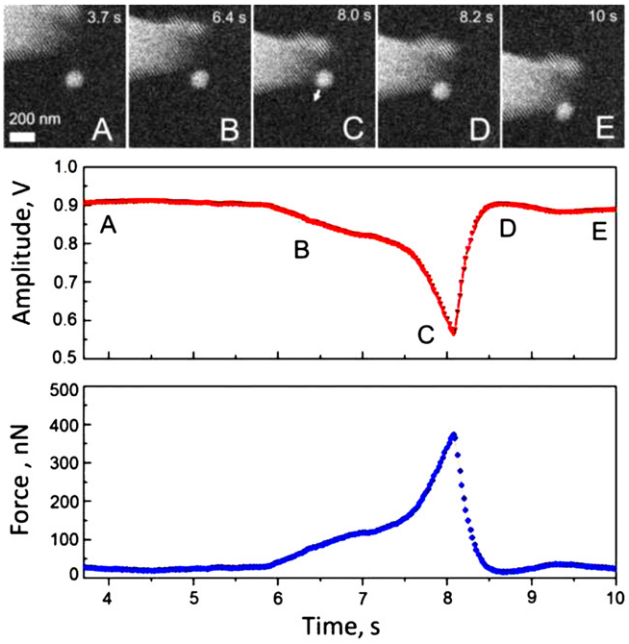

Fig. 2. Snapshots of the manipulation process and corresponding amplitude and force curves, Normal mode (sample tilt corrected).

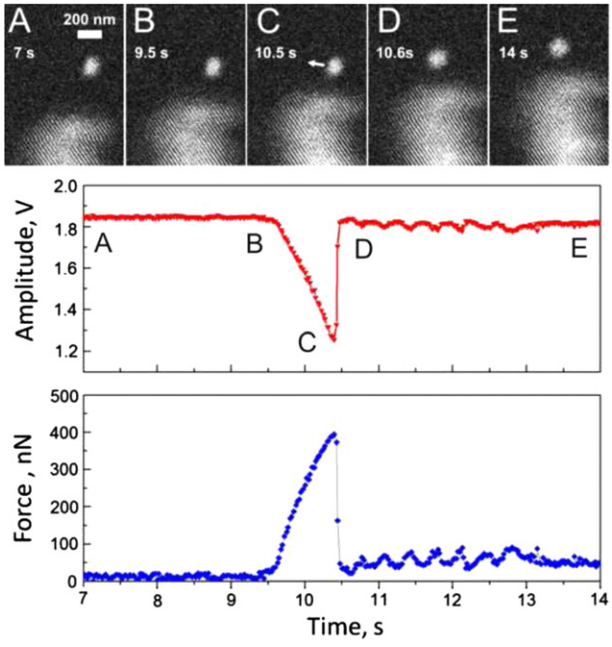

Fig. 3. Snapshots of the manipulation process and corresponding amplitude and force curves, Shear mode.

Fig. 4 displays a distribution histogram of the static friction forces for the manipulation experiments in Normal and Shear modes. The static friction values for the cases when the amplitude dropped to zero remain unknown and thus could not be included in the histogram.

4. Discussion

From the experimental results, it is evident that considerable force is needed to overcome static friction in this system. However, once the threshold for static friction was exceeded and the particle moved smoothly with the tip, then only minor changes in oscillation amplitude were observed in a few cases. Most of kinetic

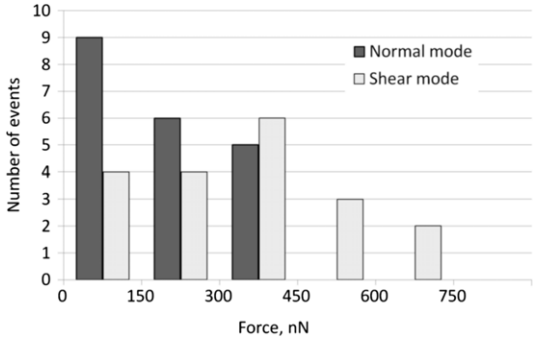

Fig. 4. Distribution of static friction forces based on 20 manipulation events in Normal mode and 17 manipulation events in Shear mode.

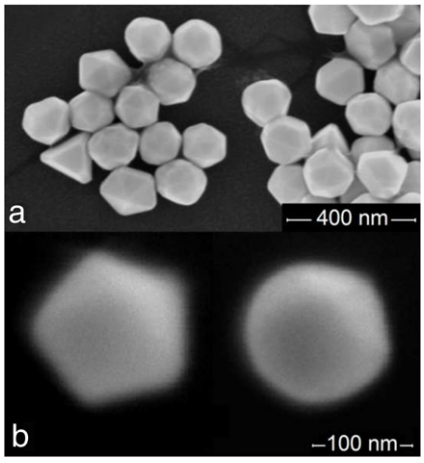

Fig. 5. (a) Au particles of different shape as deposited from solution. (b) SEM micrograph of the same Au particle before and after annealing for 1 h at 773 K.

friction values were below the detection limits of our setup. This finding is in agreement with those of other researchers, who have demonstrated that kinetic friction is vanishing for clean surfaces in vacuum [14].

Variations in the experimental values of static friction may be due to the fact that the area of contact between a particle and a substrate can vary due to deviations from a spherical shape. From Fig. 5(a) it is clearly seen that the Au particles used in the experiment were, in general, not spherical and had facets of different sizes.

Geometrical factors may also play a crucial role in the reduction of static friction after a thermal treatment. In our experiments, the main reason for heating the samples was to burn out the surfactant remaining after the deposition of the particles onto the substrate. However, it was found that annealing at 773 K also led to a rounding of the particles (see Fig. 5(b)), which, in turn, should result in reduction of the contact area and static friction.

Here, we provide an analytical estimate of the static friction considering the geometric parameters [15] of the particles used in our manipulation experiments. It has been theoretically proposed and experimentally proven that friction at the nanoscale is proportional to the contact area: $F_{frict} = \tau A$, where A is the contact area and τ is the Shear strength [16].

For spherical particles, the contact area can be calculated on the basis of continuum elasticity models for deformable spheres [4] such as the JKR model [17] or the DMT-M model [18]. According to Tabor [19], the choice of the most suitable model is determined by the parameter

$$\eta = \left(\frac{16R\gamma^2}{9K^2z_0^3}\right)^{1/3}, \quad (1)$$

Table 1
Estimated static friction forces for 150 nm Au particles of different geometries.

Shape	Contact area, nm^2	Static friction, nN
Spherical	31	9
Tetrahedral	9743	2768
Decahedral	3652	1038
Icosahedral	2693	765

where R is the radius of the sphere, γ is the work of adhesion, and z_0 is the equilibrium spacing for the Lennard-Jones potential of the surfaces. K is the combined elastic modulus of the sphere and substrate, defined as $K = 4/3[(1-\nu_1^2)/E_1 + (1-\nu_2^2)/E_2]^{-1}$ in which $\nu_{1,2}$ and $E_{1,2}$ are the Poisson ratios and Young moduli of the substrate and sphere, respectively.

Assuming the following parameters for silicon and gold: $E_1 = 71.7$ GPa, $\nu_1 = 0.17$, $E_2 = 78$ GPa, $\nu_2 = 0.44$, $\gamma = 50$ mJ/m^2 [4], $R = 75$ nm and $z_0 = 0.3$ nm, we obtained $\eta = 0.158$. For small η, the DMT-M theory is more appropriate [20]. According to the DMT-M model, the contact area

$$A_{\text{DMT-M}} = \pi \left(\frac{2\pi\gamma}{K}\right)^{2/3} R^{4/3} \tag{2}$$

for spherical Au NPs with $R = 75$ nm is $A_{\text{DMT-M}} \approx 31.43$ nm^2.

The contact areas of the faceted NPs can be easily calculated using geometrical considerations. The results of the calculations for tetrahedral, decahedral and icosahedral NPs are presented in Table 1.

The Shear strength τ can be estimated using the relation $\tau_{theo} = G* /30$ between the theoretical Shear strength and the combined Shear modulus, $G* = [(2-\nu_1)/G_1 + (2-\nu_2)/G_2]^{-1}$, where $G_{1,2} = E_{1,2}/2(1+\nu_{1,2})$ [19,21]. The ultimate static friction can then be calculated as $F_{frict} = \tau_{theo} A_{\text{DMT-M}}$.

It should be noted here that the geometry of real particles is more complex due to the presence of arbitrarily truncated edges and apexes (Fig. 5(a)). Thus, the contact areas and static frictions should generally be lower than the maximal values listed in Table 1.

According to the histograms (Fig. 4), low static friction force values prevail in the data set obtained. This finding can be interpreted as a reduction of contact area due to shape evolution towards the spherical after thermal treatment. For values beyond the upper detection limit (where the amplitude dropped to zero), the geometry was assumed to be highly faceted.

The displacement of strongly adhered particles entails the risk of their plastic deformation. As one of the main objectives of our study was to compare the Normal and Shear modes, we narrowed our measurements to the low-friction region.

Normal oscillation mode is commonly used for the AFM manipulation of nanoparticles. Considering that friction can be significantly higher at ambient conditions than in vacuum [15], our results correlate well with the previously reported static friction values of 130 nN for 15 nm Au nanoparticles on poly-L-lysine coated mica in air [22]. In many studies, the friction was estimated from the dissipated power [2,3]; however, the data obtained using such an approach do not allow for comparison with direct frictional force measurements.

In Normal mode, the sensor oscillated perpendicularly to the sample plane, producing a horizontal force component determined by the contact angle. The use of a nonzero contact angle requires sensor calibration in both the horizontal and vertical directions. However, according to our calibration data, the sensor was about ten times less sensitive in the Z (vertical) direction than in the Y (horizontal) direction. The ratio between the vertical and horizontal components of the applied force remains unknown, as it is determined by the contact angle, making interpretation of the recorded signal in the Normal mode complicated.

In the Shear mode, the tip oscillated parallel to the sample plane, and the alternating vertical component was almost absent (the small value may be due to imperfect alignment of the sensor with the sample). The force calibrations in the Y and Z directions showed the same sensitivity within the accuracy of our measurements.

The manipulation curves for both Normal and Shear oscillation modes were rather similar. However, the values of the static friction measured in the Normal mode were a few hundred nN lower than those measured in the Shear mode. This difference may be due to the contribution of the unaccounted vertical component in the Normal mode.

The Normal mode is closely related to the tapping mode and hence provides a stable set point. In the Shear mode, the tip oscillates above a certain area and it is more difficult to maintain a stable set point.

The influence of the impact velocity on the initial displacement of the particles is another challenging issue. We found that the step regime was more effective for the initial displacement of the particles than the scan regime. This might be related to the abruptness of motion in this regime; the tip strikes the particle with a much higher velocity than in the scan regime. Visual information concerning the real motion of the tip and the particle is restricted by the scanning speed of the SEM. Manipulation events in the step regime are so fast that we could see only the initial and final positions of the tip and the particle and have no data on motion in between these points.

To simulate a step event in the scan regime, the scanning speed was increased. Initial displacement of stuck particles was impossible below a certain threshold. The increase of the scan speed up to 5 μm/s enables moving the particles more easily. Moreover, while the particles were often plastically deformed and smeared along the surface in the case of a slow impact, at high tip velocities the particles moved as a rigid entity. This result suggests the possibility that the viscoelastic properties of Au particles may depend on the impact velocity; however, additional experiments are required to determine whether this is the case.

5. Conclusions

150 nm diameter Au nanoparticles were manipulated on an oxidized Si substrate inside an SEM with simultaneous force detection using a QTF-based sensor operated in Normal and Shear modes. The static friction was found to range from 40 to 450 nN for the Normal mode and from 50 to 750 nN for the Shear mode. The large variations in static friction values were attributed to differences in particle–sample contact areas associated with the shapes of the particles. The kinetic friction tended to be close to the detection limit and in most cases did not exceed several nN. Thermal treatment of Au particles for 1 h at 725 K resulted in a rounding of the particles and a corresponding decrease in the static friction.

Acknowledgements

This work was supported by the Estonian Science Foundation grants no. 8377, 8420, the Estonian research targeted project SF0180058s07, the Doctoral School of Functional Materials and Technology, the University of Tartu, the Estonian Nanotechnology Competence Center and the ESF Fanas program "Nanoparma". The authors would like to thank Dr. K. Mougin for useful discussion, and Siim Pikker for assistance with the SEM.

References

[1] H. Ahmed, J. Vac. Sci. Technol. B 15 (1997) 2101.
[2] K. Mougin, E. Gnecco, A. Rao, M. Cuberes, S. Jayaraman, E. McFarland, H. Haidara, E. Meyer, Langmuir 24 (2008) 1577.

[3] C. Ritter, M. Heyde, B. Stegemann, K. Rademann, U.D. Schwarz, Phys. Rev. B 71 (2005) 085405.
[4] S. Kim, D.C. Ratchford, X. Li, ACS Nano 3 (2009) 2989–2994.
[5] C. Baur, A. Bugacov, B.E. Koel, A. Madhukar, N. Montoya, T.R. Ramachandran, A.A.G. Requicha, R. Resch, P. Will, Nanotechnology 9 (1998) 360.
[6] D. Dietzel, M. Feldmann, H. Fuchs, U. Schwarz, A. Schirmeisen, Appl. Phys. Lett. 95 (2009) 053104.
[7] M. Sitti, H. Hashimoto, IEEE-ASME Trans. Mech. 5 (2000) 199–211.
[8] D. Dietzel, T. Mönninghoff, L. Jansen, H. Fuchs, C. Ritter, U. Schwarz, A. Schirmeisen, J. Appl. Phys. 102 (2007) 084306.
[9] S. Rozhok, V. Chandraskekhar, Solid State Commun. 121 (2002) 683–686.
[10] A.J. Melmed, J. Vac. Sci. Technol. B 9 (1991) 601.
[11] C.T. Gibson, G.S. Watson, S. Myhra, Nanotechnology 7 (1996) 259–262.
[12] S.M. Cook, T.E. Schaffer, K.M. Chynoweth, M. Wigton, R.W. Simmonds, K.M. Lang, Nanotechnology 17 (2006) 2135–2145.
[13] J. Dietrich, Pure Appl. Geophys. 116 (1978) 790–806.
[14] D. Dietzel, C. Ritter, T. Monninghoff, H. Fuchs, A. Schirmeisen, U.D. Schwarz, Phys. Rev. Lett. 101 (2008) 125505.
[15] D. Seo, C.I. Yoo, I.S. Chung, S.M. Park, S. Ryu, H. Song, J. Phys. Chem. C 112 (2008) 2469–2475.
[16] R.W. Carpick, M. Salmeron, Chem. Rev. 97 (1997) 1163–1194.
[17] K.L. Johnson, K. Kendall, A.D. Roberts, Proc. R. Soc. A 324 (1971) 301–313.
[18] D. Maugis, J. Colloid Interface Sci. 150 (1992) 243–269.
[19] S.P. Timoshenko, J.N. Goodier, Theory of Elasticity, McGraw-Hill, New York, 1987.
[20] D. Tabor, J. Colloid Interface Sci. 58 (1977) 2–13.
[21] A.H. Cottrell, Dislocations and Plastic Flow in Crystals, Oxford University Press, Oxford, UK, 1953.
[22] R. Resch, C. Baur, A. Bugacov, B.E. Koel, A. Madhukar, A.A.G. Requicha, P. Will, Appl. Phys. A 67 (1998) 265–271.